

Magnetic reconnection, plasmoids and numerical resolution

José María García Morillo & Alexandros Alexakis^{1†}

Laboratoire de Physique de l'Ecole Normale Supérieure, ENS, Université PSL, CNRS, Sorbonne Université, Université Paris-Diderot, Sorbonne Paris Cité, Paris, France

(Received xx; revised xx; accepted xx)

Explaining fast magnetic reconnection in electrically conducting plasmas has been a theoretical challenge in plasma physics since its first description by Eugene N. Parker. In the recent years the observed reconnection rate has been shown by numerical simulations to be explained by the plasmoid instability that appears in highly conductive plasmas. In this work we show that the plasmoid instability is very sensitive to the numerical resolution used. It is shown that well resolved runs display no plasmoid instability even at Lundquist number as large as $5 \cdot 10^5$ achieved at resolutions of 32768^2 grid points. On the contrary in simulations that are under-resolved below a threshold, the plasmoid instability manifests itself with the formation of larger plasmoids the larger the under-resolving is. The present results thus question the description of the plasmoid instability as a mechanism for fast magnetic reconnection.

1. Introduction

Magnetic reconnection refers to the sudden change of magnetic topology due to Ohmic dissipation or other micro-scale plasma processes. In astrophysics it is met in solar flares, coronal mass ejections, the solar wind and the Earth's magnetosphere to mention a few examples. In laboratory scales it is observed in tokamak discharges, and in reversed field pinch devices. It is responsible for the fast acceleration of charged particles and plasma heating Yamada *et al.* (2010). It was noted early on Giovanelli (1946) that the rate of reconnection observed in astrophysical plasmas was much faster than the relevant Ohmic time scale. The model of Sweet and Parker (Parker 1957; Sweet 1958) improved on this estimate by introducing what is now known as the Sweet-Parker model where the reconnection timescale is accelerated by a factor of $\sqrt{S_L}$ where S_L stands for the Lundquist number defined as $S_L = V_A L / \eta$ where V_A is the Alfvén speed, L the typical structure size and η the magnetic diffusivity. Although the Lundquist number in astrophysical plasmas is large, the improvement of the Sweet-Parker model still lacks orders of magnitude compared to observations. Different, explanations have been put forward to produce faster reconnection rates than the Sweet-Parker model including different geometry of the layer (Petschek 1964), Hall effect (Morales *et al.* 2005; Wang *et al.* 2000), Electron pressure (Egedal *et al.* 2013; Wang *et al.* 2000), Electron inertia (Andrés *et al.* 2014) and turbulence (Lazarian *et al.* 2015, 2020). However even without adding additional physics it has been argued that a two dimensional magnetohydrodynamic (2D-MHD) model as the one proposed by Sweet-Parker can result in *fast* (*ie* magnetic diffusivity independent) reconnection rate if the Lundquist number is large enough so that the plasmoid instability develops (Shibata & Tanuma 2001). The plasmoid instability appears for $S_L \gtrsim 10^4$ (Loureiro *et al.* 2007; Samtaney *et al.* 2009)

† Email address for correspondence: alexakis@phys.ens.fr

and leads to the formation of magnetic islands along the current sheet that enhance the reconnection rate (Lapenta 2008; Bhattacharjee *et al.* 2009; Samtaney *et al.* 2009; Daughton *et al.* 2009; Cassak *et al.* 2009; Huang & Bhattacharjee 2010, 2012; Loureiro *et al.* 2013; Huang & Bhattacharjee 2013; Loureiro *et al.* 2012; Uzdensky *et al.* 2010). These results were based on extended numerical simulations using a variety of codes including particle in cell methods, finite volume and pseudospectral methods. We argue however in this work that reconnection is particularly sensitive to the numerical resolution and some of these results would need to be reexamined.

2. Numerical model

In this work we revisit the reconnection problem in 2D-MHD paying particular emphasis on numerical convergence. We consider the 2D-MHD equations in a double periodic square box of size $L = 2\pi$. In terms of vorticity and the magnetic vector potential they read:

$$\partial_t \omega + \mathbf{u} \cdot \nabla \omega = \mathbf{b} \cdot \nabla j + \nu \nabla^2 \omega \quad (2.1)$$

$$\partial_t a + \mathbf{u} \cdot \nabla a = \eta \nabla^2 a \quad (2.2)$$

where $\omega = \mathbf{e}_z \cdot \nabla \times \mathbf{u}$ is the vorticity with \mathbf{e}_z the direction perpendicular to the examined plane and \mathbf{u} the velocity field. The magnetic field is given by $\mathbf{b} = \nabla \times (\mathbf{e}_z a)$ where $\mathbf{e}_z a$ is the magnetic vector potential. The current along \mathbf{e}_z is given by $j = \mathbf{e}_z \cdot \nabla \times \mathbf{b} = -\nabla^2 a$. The viscosity ν is set equal to the magnetic diffusivity η for all our simulations. As initial conditions we consider the Orsang-Tang vortex (Orszag & Tang 1979) plus a small perturbation:

$$a(t = 0, \mathbf{x}) = A_0[-\cos(x) + \cos(2y)/2] + a_p \quad (2.3)$$

while the velocity field is defined by its stream function ψ (such that $u_x = \partial_y \Psi$ and $u_y = -\partial_x \Psi$) by

$$\Psi(t = 0, \mathbf{x}) = \Psi_0 \sin(x) \sin(y) + \psi_p. \quad (2.4)$$

The amplitudes A_0 and Ψ_0 are such that the initial magnetic energy density is $\frac{1}{2} \langle |\mathbf{b}|^2 \rangle = \frac{1}{2}$ and the kinetic energy is $\frac{1}{2} \langle |\mathbf{u}|^2 \rangle = \frac{1}{8}$. The perturbations a_p, ψ_p are chosen to include Fourier modes with wavenumber $|\mathbf{k}| < 16$ with random phases and their amplitude are such that their energy corresponds to 0.25% of the total energy. They provide a seed for linear instabilities to develop that otherwise would depend on the the round-off error. A visualisation of the initial conditions in terms of the current square is shown in the left panel of figure 1.

The equations were solved using the GHOST pseudospectral code (Mininni *et al.* 2011) with a 4th order Runge-Kutta scheme for the time advancement, the 2/3 rule for de-aliasing and using a uniform grid of N grid points in each direction. Many different numerical simulations were carried out varying the resolution and the value of $\eta = \nu$. The parameters of all our runs are given in the table 1.

The evolution of the system leads to the formation of a current sheet aligned along the x -axis centered at $x = 0$. The intensity of the current sheet measured by the mean current density squared $\langle j^2 \rangle$ increases rapidly and peaks at a time around $t \simeq 1.9$ after which it decays. In what follows all the studies are performed at the peak of $\langle j^2 \rangle$. At this time we define the Lundquist number as $S_L \equiv B_{max}/(\eta k_1)$ where $k_1 = 1$ is the smallest non-zero wavenumber. To calculate B_{max} for each y we calculate the mean magnetic field $\bar{b}_x(y)$ along the x direction in the range $x \in [-\pi/8, \pi/8]$ (shown by the horizontal green line in figure 1). B_{max} is then defined as the first local maximum of $\bar{b}_x(y)$ as one moves away

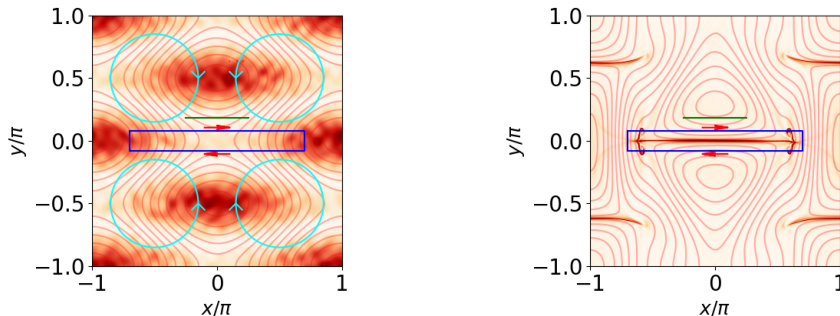


Figure 1: Visualisation of the current density of the initial conditions and the resulting current layer in the entire domain. Red lines, indicate the magnetic field lines while blue lines indicate the velocity field. The blue box marks the zoomed in region that is shown in the subsequent figures.

N	η	S_L	N	η	S_L	N	η	S_L
1024	0.50E-01	0.19E+02	2048	0.20E-02	0.12E+04	4096	0.15E-04	0.14E+06
1024	0.20E-01	0.70E+02	2048	0.10E-02	0.26E+04	4096	0.70E-05	0.35E+06
1024	0.10E-01	0.18E+03	2048	0.50E-03	0.54E+04	4096	0.50E-05	0.46E+06
1024	0.50E-02	0.41E+03	2048	0.20E-03	0.15E+05	4096	0.20E-05	0.91E+06
1024	0.20E-02	0.12E+04	2048	0.10E-03	0.30E+05	4096	0.10E-05	0.18E+07
1024	0.10E-02	0.26E+04	2048	0.50E-04	0.61E+05	8192	0.50E-04	0.62E+05
1024	0.50E-03	0.54E+04	2048	0.20E-04	0.13E+06	8192	0.15E-04	0.18E+06
1024	0.20E-03	0.15E+05	2048	0.15E-04	0.17E+06	8192	0.10E-04	0.28E+06
1024	0.10E-03	0.30E+05	2048	0.50E-05	0.24E+06	8192	0.50E-05	0.51E+06
1024	0.50E-04	0.47E+05	2048	0.30E-05	0.39E+06	8192	0.25E-05	0.95E+06
1024	0.30E-04	0.59E+05	2048	0.20E-05	0.58E+06	8192	0.20E-05	0.12E+07
1024	0.20E-04	0.87E+05	2048	0.15E-05	0.75E+06	8192	0.10E-05	0.23E+07
1024	0.15E-04	0.10E+06	2048	0.10E-05	0.14E+07	16384	0.10E-04	0.28E+06
1024	0.10E-04	0.14E+06	4096	0.20E-03	0.15E+05	16384	0.50E-05	0.39E+06
1024	0.70E-05	0.16E+06	4096	0.10E-03	0.30E+05	16384	0.25E-05	0.86E+06
1024	0.50E-05	0.23E+06	4096	0.50E-04	0.62E+05	32768	0.50E-05	0.54E+06
1024	0.15E-05	0.61E+06	4096	0.30E-04	0.11E+06			

Table 1: Simulation parameters N, η, S_L . Boldface N is used for well-resolved and marginally well resolved runs.

from the current sheet at $y = 0$. The non-dimensional reconnection rate is defined here as $RR = u_{in}/B_{max}$ where u_{in} is again calculated by finding the mean inwards velocity $-\overline{u}_y(y)$ over the same segment as for $\overline{b}_x(y)$ and then u_{in} is defined as the first maximum of $-\overline{u}_y(y)$ as one moves away from the current layer. Note that this average is crucial in the presence of plasmoids that make local values of u_y and b_x fluctuate strongly.

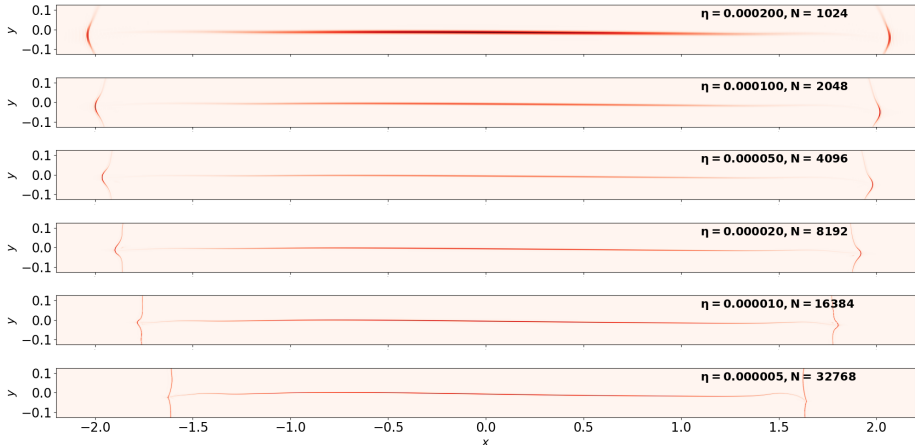


Figure 2: Squared current density for well resolved runs (zoomed in the current layer) for different values of η taken from the marginally well resolved runs. The visualised domain corresponds to the blue box shown in figure 1.

3. Results

Exact solutions of reconnection layers describing the formation of the reconnection are not feasible and one needs to rely on numerical solutions. For the validity of a numerical method to be verified one needs to demonstrate that for a given set of physical parameters there exists a resolution N_c such that all larger resolutions $N > N_c$ give the same result, up to a small error that can be bounded by a decreasing function of N . Such a procedure proves that the numerical solution does not depend on the resolution and approaches the exact solution of the problem. Different numerical methods have different convergence rates. Finite difference and finite volume codes lead to a power-law convergence implying that the error made decreases as a negative power-law as $N > N_c$ is increased, while pseudo-spectral and finite element codes result in an exponential convergence. This exponential convergence can be realised by considering the energy spectrum of the involved fields here defined as $E_b(k) = \frac{1}{2} \sum_{k < |\mathbf{q}| \leq k+1} |\tilde{\mathbf{b}}_{\mathbf{q}}|^2$ where $\tilde{\mathbf{b}}_{\mathbf{q}}$ is the Fourier transform of the magnetic field \mathbf{b} . Similarly, the squared current spectrum is defined as $E_J(k) = k^2 E_b(k)$. For a smooth field the energy and current spectrum display an exponential decrease with the wavenumber at large k . Further increase of resolution thus adds exponentially small corrections. In the present study we have considered that a simulation is well resolved if the peak of the squared current spectrum defined as $E_J(k) = k^2 E_b(k)$ is at least ten times larger than its value at $k = k_{max} = N/3$ the maximum allowed wavenumber ie $\max_k \{E_J(k)\} \geq 10 E_J(k_{max})$. This implies that most of the Ohmic dissipation is correctly captured. The consequences of violating this criterion are severe.

In figure 2 we show visualisations of the squared current density (zoomed in the current layer) obtained from well resolved runs for different values of η . None of these runs displayed visible plasmoids even though values of $S_L = 5.4 \cdot 10^5$ are reached. We note that the current layer is not straight. Instabilities have developed that have given a bent shape of the current layer but have not led to plasmoid formation.

In figure 3 we plot the squared current density again for the smallest value of η examined for different resolutions N . From these runs only the last one for $N = 32768$ is well resolved based on the criterion mentioned before. It is striking that all under-

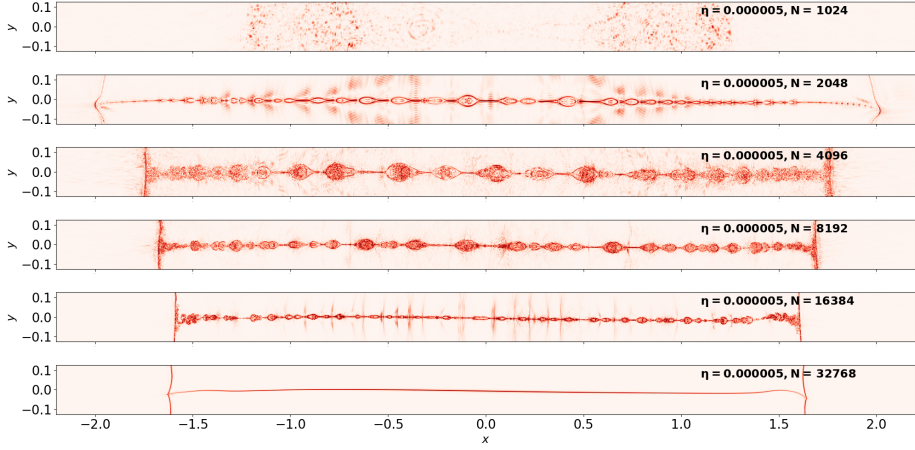


Figure 3: Squared current density for the smallest value of η examined (zoomed in the current layer) for different resolutions N .

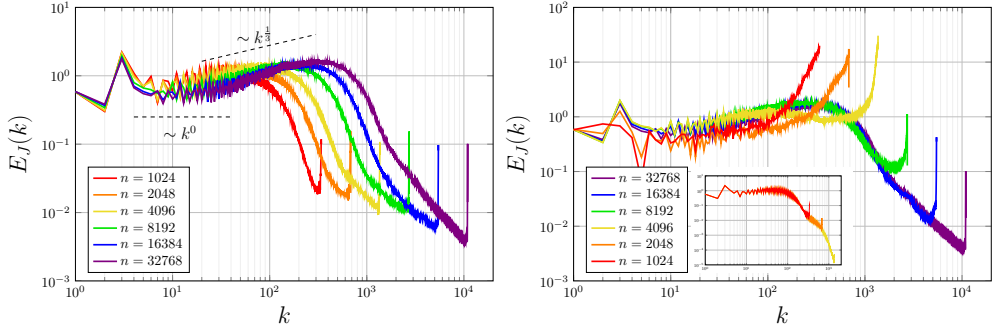


Figure 4: Squared current density spectra corresponding to the runs shown in figures 2 (left) and 3 (right).

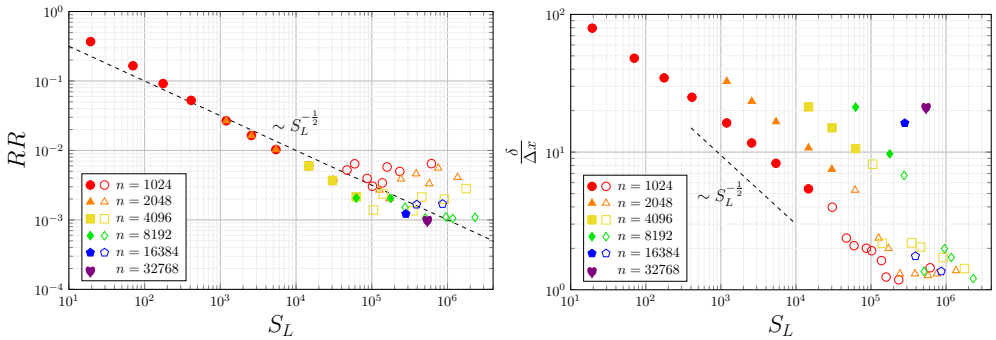


Figure 5: Left panel: Reconnection rate as a function of S_L for all runs well-resolved (filled symbols) and under-resolved (open symbols). Right panel: Width of the reconnection layer normalised by the grid size as function of S_L .

resolved runs displayed plasmoids. In fact the worst the under-resolving the largest the plasmoids appear. This phenomenon is also present at smaller values of η examined: when the well-resolved criterion is violated plasmoids are present. Table 1 shows the parameters used for all runs (not just the ones shown in figures 2 and 3) indicating the value of resolution N required for each value of η so that the simulation is well resolved. All resolutions smaller than the marked value displayed plasmoids. Similar features due to under-resolving have also been observed in Burger’s turbulence and the Navier-stokes where they have been studied extensively (Ray *et al.* 2011; Murugan & Ray 2023).

Further insight can be gained by looking at the energy spectra. The left panel of figure 4 shows the the current density spectra for the runs corresponding to figure 2, while the right panel of the same figure, shows the spectra for the runs corresponding to figure 3. In the left panel all runs are marginally well resolved. As resolution is increased and η is decreased $E_J(k)$ progresses to larger wavenumbers forming a k^0 power-law range that reflects the approximate discontinuity of the magnetic field in the current sheet. This power-law range is followed by an increase that could be attributed to either bottleneck (Falkovich 1994; Donzis & Sreenivasan 2010; Agrawal *et al.* 2020) or a transition to two dimensional turbulence as a result of the instabilities that have developed with $E(k) \propto k^{-5/3}$. At larger wavenumbers the spectrum shows a steep exponential decrease. Finally at the highest wavenumbers near k_{\max} there is a sharp increase. This is a numerical artifact due to the sharp spectral truncation that leads to a partial thermalisation of the high wavenumbers (Cichowlas *et al.* 2005; Alexakis & Brachet 2020). Further increasing the resolution for a given value of η has little effect as is demonstrated in the inset of the right panel where the well-resolved run for $N = 1024$ (plotted in the left panel) is repeated at larger resolutions $N = 2048$ and $N = 4096$.

The behavior described above changes when the resolution criterion is not satisfied. In the right panel of fig. 4, where only the simulation with the largest N is well-resolved, clear under-resolving features can be testified. As the resolution is decreased the amount of energy at the largest wavenumbers increases changing the shape of the spectrum. It is worth noting that the integral of $E_J(k)$ is proportional to the Ohmic dissipation and even at the second to largest resolution $N = 16384$ the Ohmic dissipation due to the wavenumbers at k_{\max} is comparable to the dissipation due to the peak of $E_J(k)$ around $k = 500$. It is thus not surprising that violating the well resolved criterion mention before can lead to erroneous estimates of the reconnection rate and appearance of plasmoids.

This is clearly demonstrated in figure 5 where the reconnection rate RR is plotted as a function of S_L for all our simulations. Filled symbols correspond to well resolved runs while open symbols correspond to under-resolved runs. All well resolved runs display the Sweet-Parker scaling $RR \propto S_L^{-1/2}$ even up to $S_L = 5 \cdot 10^5$ that corresponds to the run at $N = 32768$. When the runs are under-resolved however deviations from this scaling appear, leading to a S_L -independent scaling. This however is a numerical artifact. The reason can be linked to the thickness of the current sheet. In the right panel we plot the thickness of the current layer defined as $\delta \equiv B_{\max}/j_{\max}$ normalised by the grid size $\Delta x = 2\pi/N$ for all runs as well. Well resolved runs follow again the Sweet-Parker prediction $\delta \propto S_L^{-1/2}$ but this scaling obviously ceases to be true when the width of the current sheet is comparable to the grid size.

4. Conclusions

Reconnection is a topological change of field lines that can only be broken by micro-scale processes. Under-resolving can be one of these processes although not a physical

one. It is hard to imagine that continuity of field lines can be preserved when the finiteness of the grid size is apparent. Thus care needs to be taken when topological changes are studied with numerical codes. The present results indicate that some of the conclusions for magnetic reconnection due to plasmoids in 2D MHD need to be re-evaluated. We note however that other mechanisms that can lead to a change of field line topology as the ones mentioned in the introduction can provide seed to lead to the formation of plasmoids.

This work was granted access to the HPC resources of GENCI-TGCC & GENCI-CINES (Project No. A0130506421, A0150506421). This work has also been supported by the Agence Nationale de la Recherche (ANR project DYSTURB No. ANR-17-CE30-0004 and LASCATURB No. ANR-23-CE30).

REFERENCES

- AGRAWAL, RAHUL, ALEXAKIS, ALEXANDROS, BRACHET, MARC E & TUCKERMAN, LAURETTE S 2020 Turbulent cascade, bottleneck, and thermalized spectrum in hyperviscous flows. *Physical Review Fluids* **5** (2), 024601.
- ALEXAKIS, ALEXANDROS & BRACHET, MARC-ETIENNE 2020 Energy fluxes in quasi-equilibrium flows. *Journal of Fluid Mechanics* **884**, A33.
- ANDRÉS, NAHUEL, MARTIN, LUIS, DMITRUK, PABLO & GÓMEZ, DANIEL 2014 Effects of electron inertia in collisionless magnetic reconnection. *Physics of Plasmas* **21** (7).
- BHATTACHARJEE, A, HUANG, YI-MIN, YANG, H & ROGERS, B 2009 Fast reconnection in high-lundquist-number plasmas due to the plasmoid instability. *Physics of Plasmas* **16** (11).
- CASSAK, PA, SHAY, MA & DRAKE, JF 2009 Scaling of sweet-parker reconnection with secondary islands. *Physics of Plasmas* **16** (12).
- CICHOWLAS, CYRIL, BONAÏTI, PAULINE, DEBBASCH, FABRICE & BRACHET, MARC 2005 Effective dissipation and turbulence in spectrally truncated euler flows. *Physical Review Letters* **95** (26), 264502.
- DAUGHTON, WILLIAM, ROYTERSHEYN, VADIM, ALBRIGHT, BJ, KARIMABADI, HOMA, YIN, LIN & BOWERS, KEVIN J 2009 Transition from collisional to kinetic regimes in large-scale reconnection layers. *Physical Review Letters* **103** (6), 065004.
- DONZIS, DA & SREENIVASAN, KR 2010 The bottleneck effect and the kolmogorov constant in isotropic turbulence. *Journal of fluid mechanics* **657**, 171–188.
- EGEDAL, JAN, LE, ARI & DAUGHTON, WILLIAM 2013 A review of pressure anisotropy caused by electron trapping in collisionless plasma, and its implications for magnetic reconnection. *Physics of Plasmas* **20** (6).
- FALKOVICH, GREGORY 1994 Bottleneck phenomenon in developed turbulence. *Physics of Fluids* **6** (4), 1411–1414.
- GIOVANELLI, RG 1946 A theory of chromospheric flares. *Nature* **158** (4003), 81–82.
- HUANG, YI-MIN & BHATTACHARJEE, A 2010 Scaling laws of resistive magnetohydrodynamic reconnection in the high-lundquist-number, plasmoid-unstable regime. *Physics of Plasmas* **17** (6).
- HUANG, YI-MIN & BHATTACHARJEE, A 2012 Distribution of plasmoids in high-lundquist-number magnetic reconnection. *Physical Review Letters* **109** (26), 265002.
- HUANG, YI-MIN & BHATTACHARJEE, A 2013 Plasmoid instability in high-lundquist-number magnetic reconnection. *Physics of Plasmas* **20** (5).
- LAPENTA, GIOVANNI 2008 Self-feeding turbulent magnetic reconnection on macroscopic scales. *Physical Review Letters* **100** (23), 235001.
- LAZARIAN, ALEX, EYINK, G, VISHNIAC, E & KOWAL, GRZEGORZ 2015 Turbulent reconnection and its implications. *Philosophical Transactions of the Royal Society A: Mathematical, Physical and Engineering Sciences* **373** (2041), 20140144.
- LAZARIAN, ALEX, EYINK, GREGORY L, JAFARI, AMIR, KOWAL, GRZEGORZ, LI, HUI, XU, SIYAO & VISHNIAC, ETHAN T 2020 3d turbulent reconnection: Theory, tests, and astrophysical implications. *Physics of Plasmas* **27** (1).

- LOUREIRO, NF, SAMTANEY, RAVI, SCHEKOCHIHIN, AA & UZDENSKY, DA 2012 Magnetic reconnection and stochastic plasmoid chains in high-lundquist-number plasmas. *Physics of Plasmas* **19** (4).
- LOUREIRO, NF, SCHEKOCHIHIN, AA & COWLEY, SC 2007 Instability of current sheets and formation of plasmoid chains. *Physics of Plasmas* **14** (10).
- LOUREIRO, NF, SCHEKOCHIHIN, AA & ZOCCO, A 2013 Fast collisionless reconnection and electron heating in strongly magnetized plasmas. *Physical Review Letters* **111** (2), 025002.
- MININNI, PABLO D, ROSENBERG, DUANE, REDDY, RAGHU & POUQUET, ANNICK 2011 A hybrid mpi–openmp scheme for scalable parallel pseudospectral computations for fluid turbulence. *Parallel computing* **37** (6-7), 316–326.
- MORALES, LAURA F, DASSO, SERGIO & GÓMEZ, DANIEL O 2005 Hall effect in incompressible magnetic reconnection. *Journal of Geophysical Research: Space Physics* **110** (A4).
- MURUGAN, SUGAN DURAI & RAY, SAMRIDDI SANKAR 2023 Genesis of thermalization in the three-dimensional, incompressible, galerkin-truncated euler equation. *Physical Review Fluids* **8** (8), 084605.
- ORSZAG, STEVEN A & TANG, CHA-MEI 1979 Small-scale structure of two-dimensional magnetohydrodynamic turbulence. *Journal of Fluid Mechanics* **90** (1), 129–143.
- PARKER, EUGENE N 1957 Sweet’s mechanism for merging magnetic fields in conducting fluids. *Journal of Geophysical Research* **62** (4), 509–520.
- PETSCHEK, HARRY E 1964 Magnetic field annihilation. In *Proceedings of a Symposium Held at the Goddard Space Flight Center, Greenbelt, Maryland, October 28-30, 1963*, , vol. 50, p. 425. Scientific and Technical Information Division, National Aeronautics and . . .
- RAY, SAMRIDDI SANKAR, FRISCH, URIEL, NAZARENKO, SERGEI & MATSUMOTO, TAKESHI 2011 Resonance phenomenon for the galerkin-truncated burgers and euler equations. *Physical Review E* **84** (1), 016301.
- SAMTANEY, R, LOUREIRO, NF, UZDENSKY, DA, SCHEKOCHIHIN, AA & COWLEY, SC 2009 Formation of plasmoid chains in magnetic reconnection. *Physical Review Letters* **103** (10), 105004.
- SHIBATA, KAZUNARI & TANUMA, SYUNITI 2001 Plasmoid-induced-reconnection and fractal reconnection. *Earth, Planets and Space* **53** (6), 473–482.
- SWEET, PA 1958 Electromagnetic phenomena in cosmical physics. In *IAU Symp. 6*, , vol. 123. Kluwer Academic Publishers.
- UZDENSKY, DA, LOUREIRO, NF & SCHEKOCHIHIN, AA 2010 Fast magnetic reconnection in the plasmoid-dominated regime. *Physical Review Letters* **105** (23), 235002.
- WANG, XIAOGANG, BHATTACHARJEE, A & MA, ZW 2000 Collisionless reconnection: Effects of hall current and electron pressure gradient. *Journal of Geophysical Research: Space Physics* **105** (A12), 27633–27648.
- YAMADA, MASAOKI, KULSRUD, RUSSELL & JI, HANTAO 2010 Magnetic reconnection. *Reviews of modern physics* **82** (1), 603.